SITE CHARACTERIZATION REPORT

SARC: Ardon, Commune (VS)

Vincent Perron, Manuel Hobiger, Donat Fäh

Last Modification: 23th August, 2021

Schweizerischer Erdbebendienst (SED)
Service Sismologique Suisse
Servizio Sismico Svizzero
Servizi da Terratrembels Svizzer

vincent.perron@sed.ethz.ch
ETH Zürich
Sonneggstrasse 5
8092 Zürich
Schweiz

Contents

Summary

Ardon (VS), located in the south of Switzerland, was selected as site for the installation of a new station, called SARC, as part of the renewal project of the Swiss Strong Motion Network (SSMNet). In order to better assess the local underground, we performed site characterization measurements with different techniques. The results of the horizontal-to-vertical spectral ratio (H/V) show curves with a fundamental frequency of about 1.70 Hz, having variable amplitude, and predominant peaks at 7.0 Hz. The inversion of the passive seismic array measurements allows us to infer two main discontinuities at about 10-20 m and 80-90 m, separating an upper layer with shear-wave velocity of about 500 m/s and a layer with velocity of about 850 m/s. At depths below 90 m, the velocity jumps to 1600-1900 m/s, possibly related to the presence of a hard rock layer. The V_{S30} value of the site is about 633 m/s, corresponding to soil class B in both EC8 and SIA261. The theoretical shear-wave transfer functions predict an amplification between 1 and 30 Hz. The maximum amplification is a factor of 2.5 at about 7 Hz. It is in good agreement with the earthquake observation for this site.

1 Introduction

The station SARC is part of the Swiss Strong Motion Network (SSMNet). The station was installed on 29 May 2018 in the framework of the second phase of the Swiss Strong Motion Network (SSMNet) renewal project (Fig. 1). In order to better characterize the underground of the station, we performed passive array measurements.

The site is of interest because it is located in a relatively populated area of the Rhone valley. It is at the edge of a very thick sedimentary basin of around 800 m. Its geographical location improves the network geometry and increases the coverage of the territory. A passive seismic measurement campaign was carried out on 17 October 2018 in order to characterize the soil column in terms of fundamental frequency and shear wave velocity.

The site is also of historical interest, as the clock tower of the church collapsed during an earthquake in April 1524 and the new church tower was built in 1525. The magnitude of this earthquake is today estimated as 5.8 and it figures among the list of the ten largest historical earthquakes in Switzerland. The location of the station in front of the church will help to estimate if the site effects have contributed to the tower collapse.
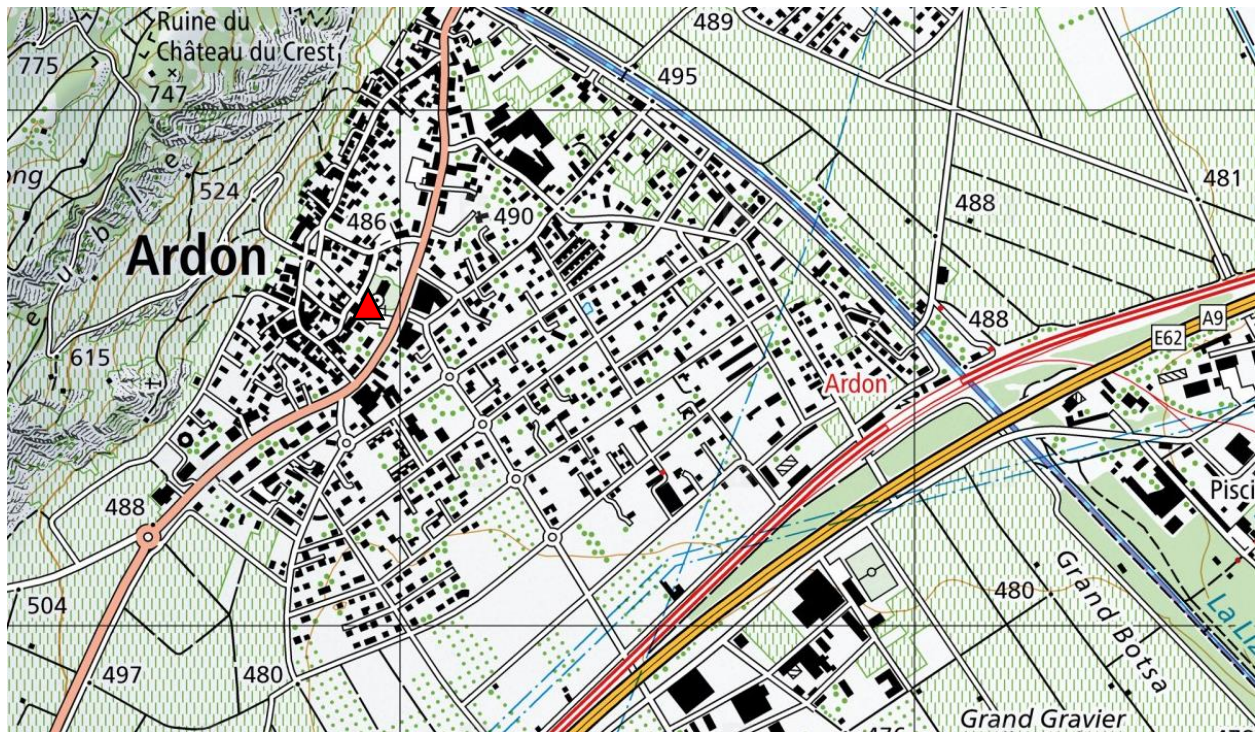

Figure 1: Map showing the location of the strong motion station SARC (red triangle) in Ardon. Source: Federal Office of Topography.

2 Geological setting

A geological map of Ardon's area is shown in Fig. 2. Station SARC is located on the edge of the basin, which is filled with alluvial deposit. The thickness of the sediments varies in the area and increases with distance from the basin's edge. This can be seen on the map of the sedimentary thickness provided by the Federal Office of Topography (see Fig 3).
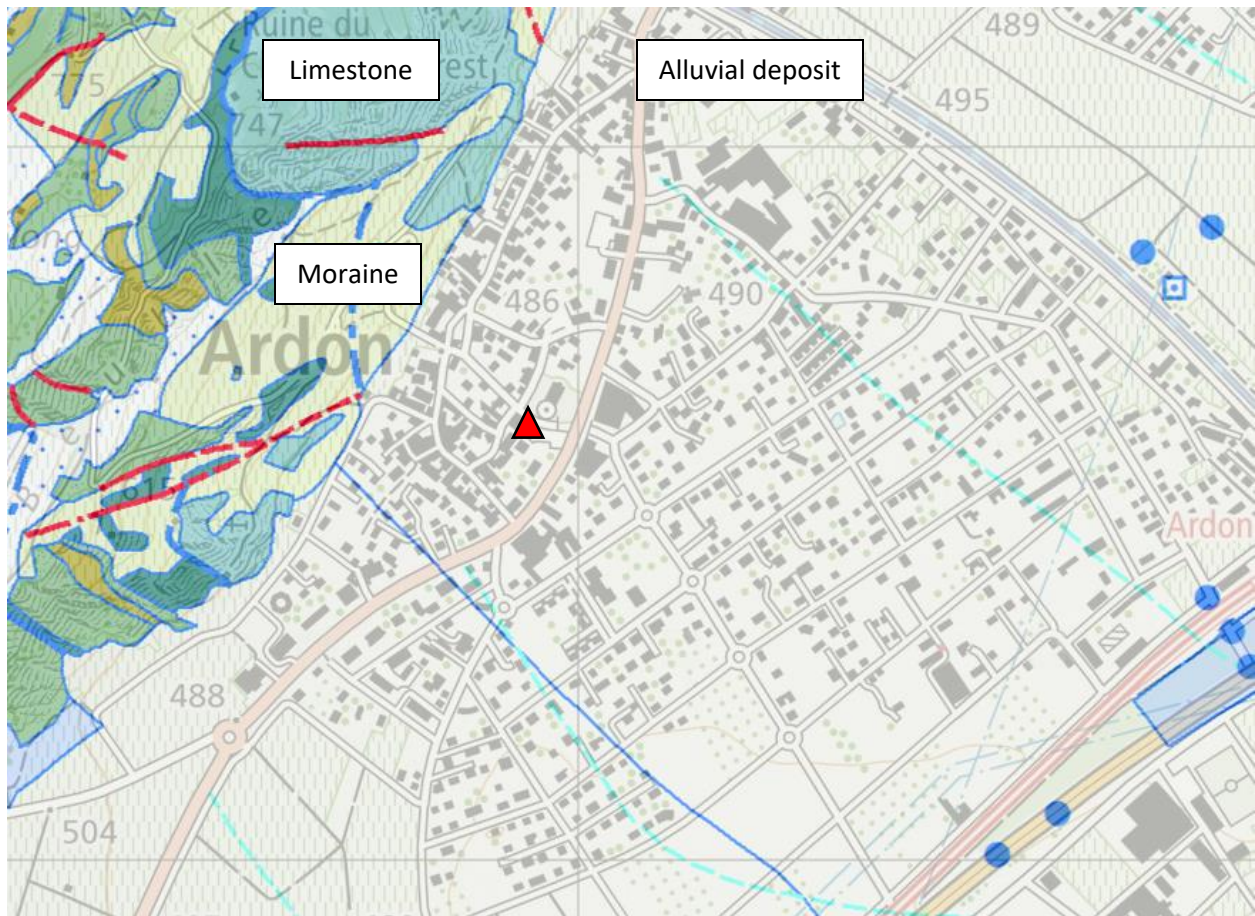
Figure 2: Geological map of the area around station SARC (red triangle). Source: Federal Office of Topography.
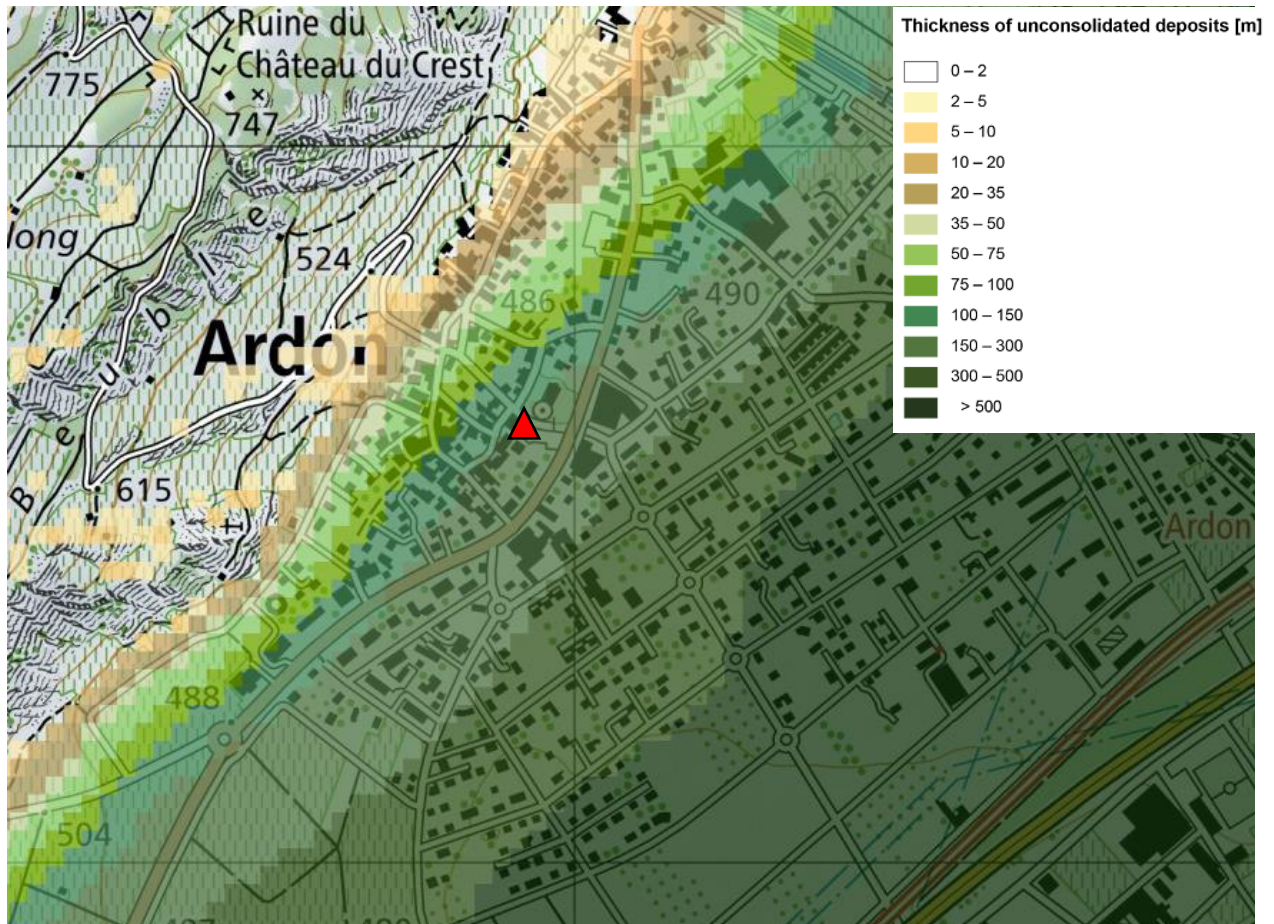
Figure 3: Map of the thickness of the sediments around station SARC. SARC is indicated by the red triangle. Source: Federal Office of Topography.

3 Station deployment and single-station analysis

3.1 Data set

To characterize the deeper underground structure around the seismic station, we performed a passive seismic measurement in October 2018 close to the location of SARC (Fig. 4 and 5).

A single array of 16 stations was installed (Fig. 5). The stations are located on five rings of three stations having different radii around the central station. These rings have radii of 8, 20, 48, 120 and 300 m. The three small rings were installed in the field using a measuring tape and a plan of the intended orientations from the central station. The accurate locations (with precision <5 cm) of the stations were estimated using a differential system (Leica Viva GS10). The minimum and maximum interstation distances in the array were 8 m and 575 m.

Each station consisted of a Lennartz 5s sensor connected to a Centaur digitizer, where four stations in the central part had two sensors connected to the same digitizer. The station names of the array are composed of "SARC" followed by a two-digit number which corresponds to the Centaur digitizer serial number for numbers lower than 60 and serial number plus 20 for higher numbers. The array recording time is 151 minutes. One sensor (SARC68) was unfortunately not recording correctly and thus unusable.

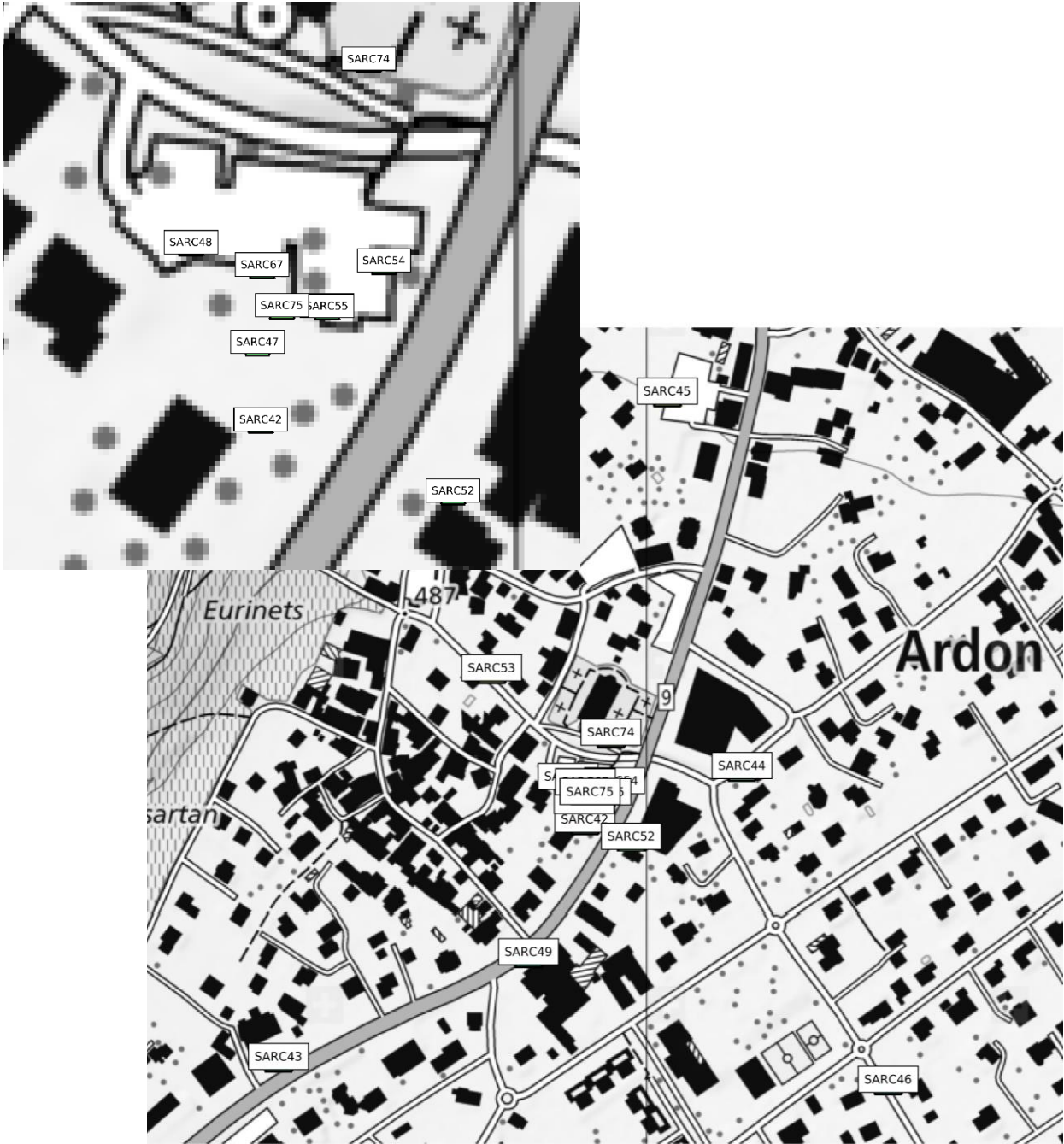*Figure 4: Seismic station installation example for the measurement in Ardon.*

Figure 5: Layout of the array measurement in Ardon. The locations of the stations for the passive seismic measurement are indicated by the station names. Source: Federal Office of Topography.

3.2 H/V and RayDec ellipticity curves

Figure 6 shows the H/V curves determined with the time-frequency analysis method (Poggi et al., 2010) and the RayDec ellipticity curves for all stations of the passive array. The curves are quite difficult to interpret because of the basin edge effects, which make the peaks very broad. However, a clear pattern is visible for stations close to the array center with a fundamental resonance frequency (f_0) of around 1.7 Hz. Figure 7 shows the map of the stations with their corresponding f_0 values. Stations of the external rings show a shift either to lower frequency for stations closer to the basin center or to higher frequency for stations close to the basin's edge (see Figs 6 and 7). There is a clear correlation between $1/f_0$ (Fig 7) and the thickness of the sediment deposit (Fig 3).
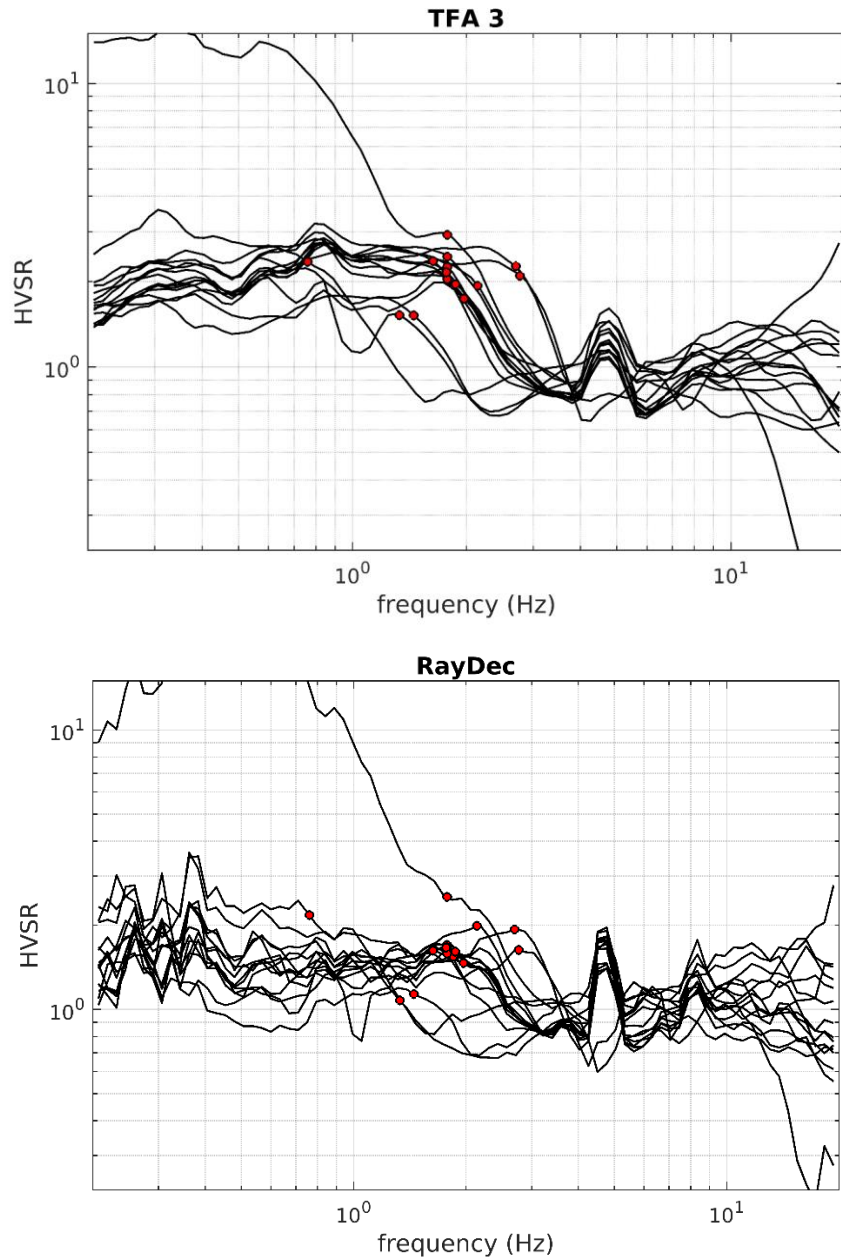

Figure 6: H/V curves (top panel) and RayDec curve (bottom panel) of the different stations of the array measurements in Ardon with picked fundamental frequency (red dot).
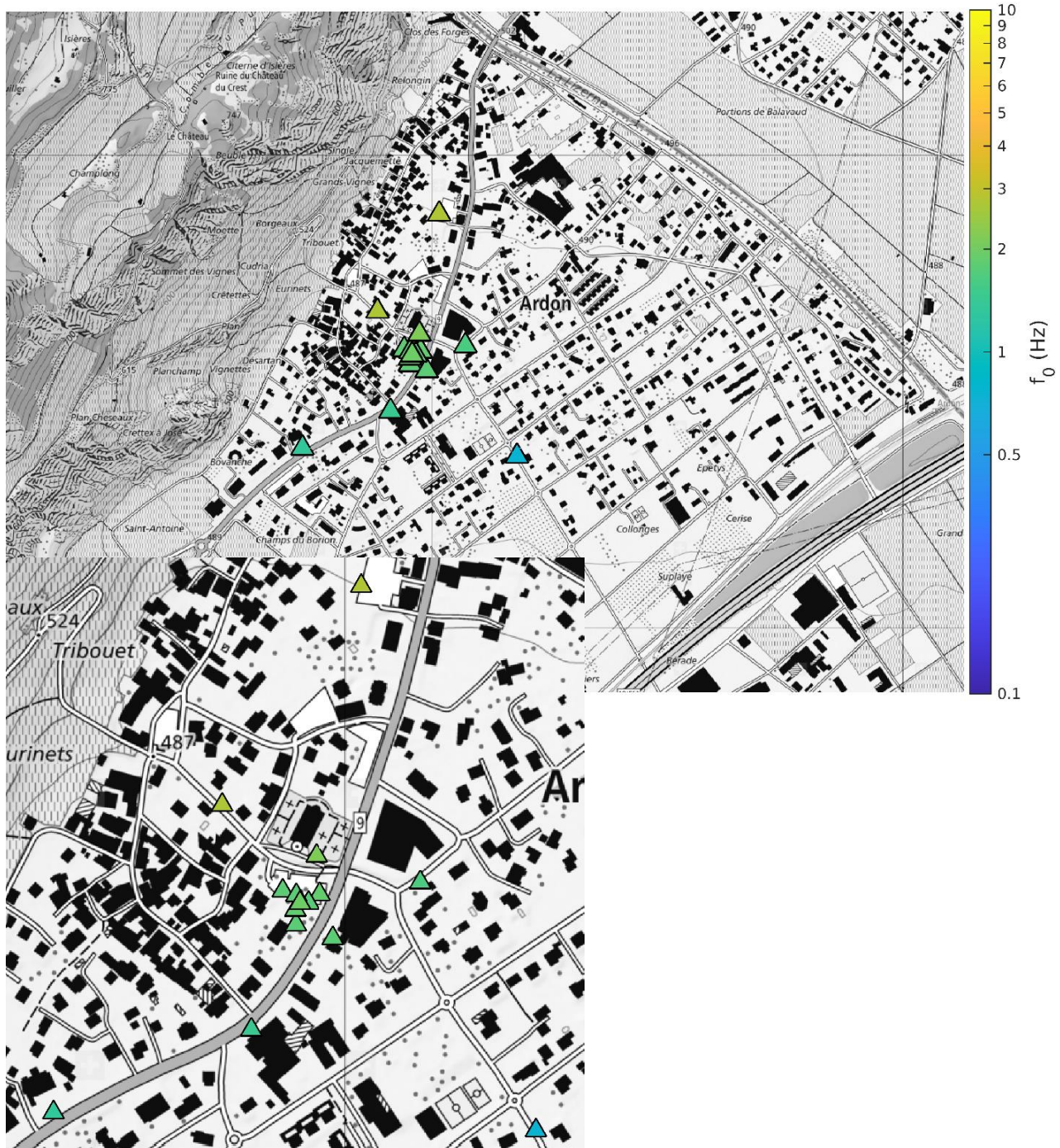
Figure 7: Layout of the array measurement in Ardon. The locations of the stations for the passive seismic measurement are indicated by the colored triangles. The color of the triangle indicates the H/V picked fundamental resonance frequency at the corresponding station. Source: Federal Office of Topography.

3.3 Polarization measurements

The polarization analysis was performed according to Burjánek et al. (2010) and Burjánek et al. (2012). The results for all stations show similarities and singularities which can be explained by local noise sources and basin-edge generated surface waves. The results for SARC48 are shown in Fig. 8. The results show that the ground motion has no pronounced 2D resonance effects. At low frequencies (<0.7 Hz), the wave field is oriented along the basin edge. At higher frequencies, no pronounced polarization directions are present, except for 1 and 5 Hz, were we can see a strong directionality effect, which is linked with an industrial source.
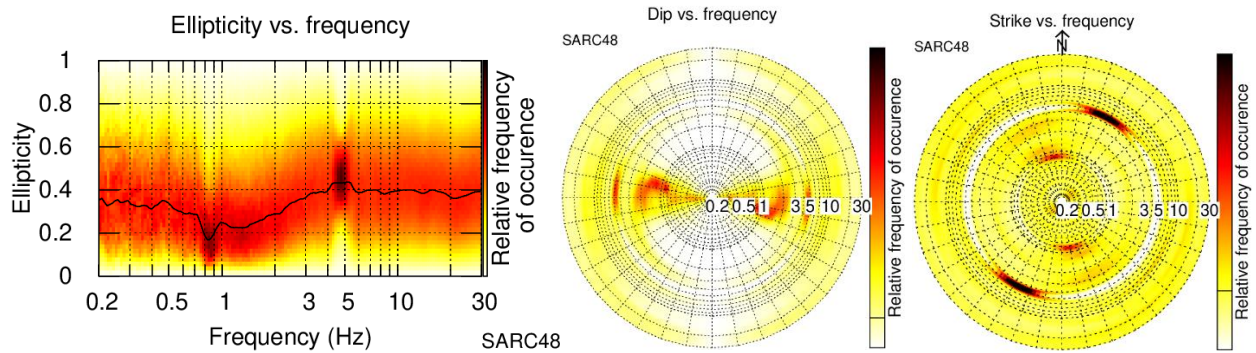

Figure 8: Polarization analysis of station SARC48.

4 Array analysis

4.1 3-component high-resolution FK (3HRFK)

The results of the 3-component high-resolution FK analysis (Poggi and Fäh, 2010) are shown in Fig. 9 for the large array (external stations – top panels), the full array (central panels) and the small array (inner station – bottom panel).

Combining the three arrays, the results on the transverse component show the dispersion curve (DC) of a single Love wave mode from 1.9 to 30 Hz. On the vertical component, corresponding to Rayleigh wave, one mode is visible from 2.5 to 24 Hz.

4.2 WaveDec

The results of the WaveDec (Maranò et al., 2012) processing are shown in Fig. 10. This technique estimates the properties of single or multiple waves simultaneously with a maximum likelihood approach. In order to get good results, the parameter γ has been tuned to modify the sharpness of the wave property estimation between purely maximum likelihood estimation and a Bayesian Information Criterion. Here, a value of $\gamma = 0.2$ was used, corresponding to a mostly maximum likelihood estimation.

Love wave dispersion curves are clearly retrieved between about 1.5 and 30 Hz. The Rayleigh wave dispersion curve can be picked between 2.3 Hz and 30 Hz.

The ellipticity angle for Rayleigh wave is given on Fig. 11. It is negative for the picked Rayleigh wave dispersion curve, corresponding to retrograde particle motion.
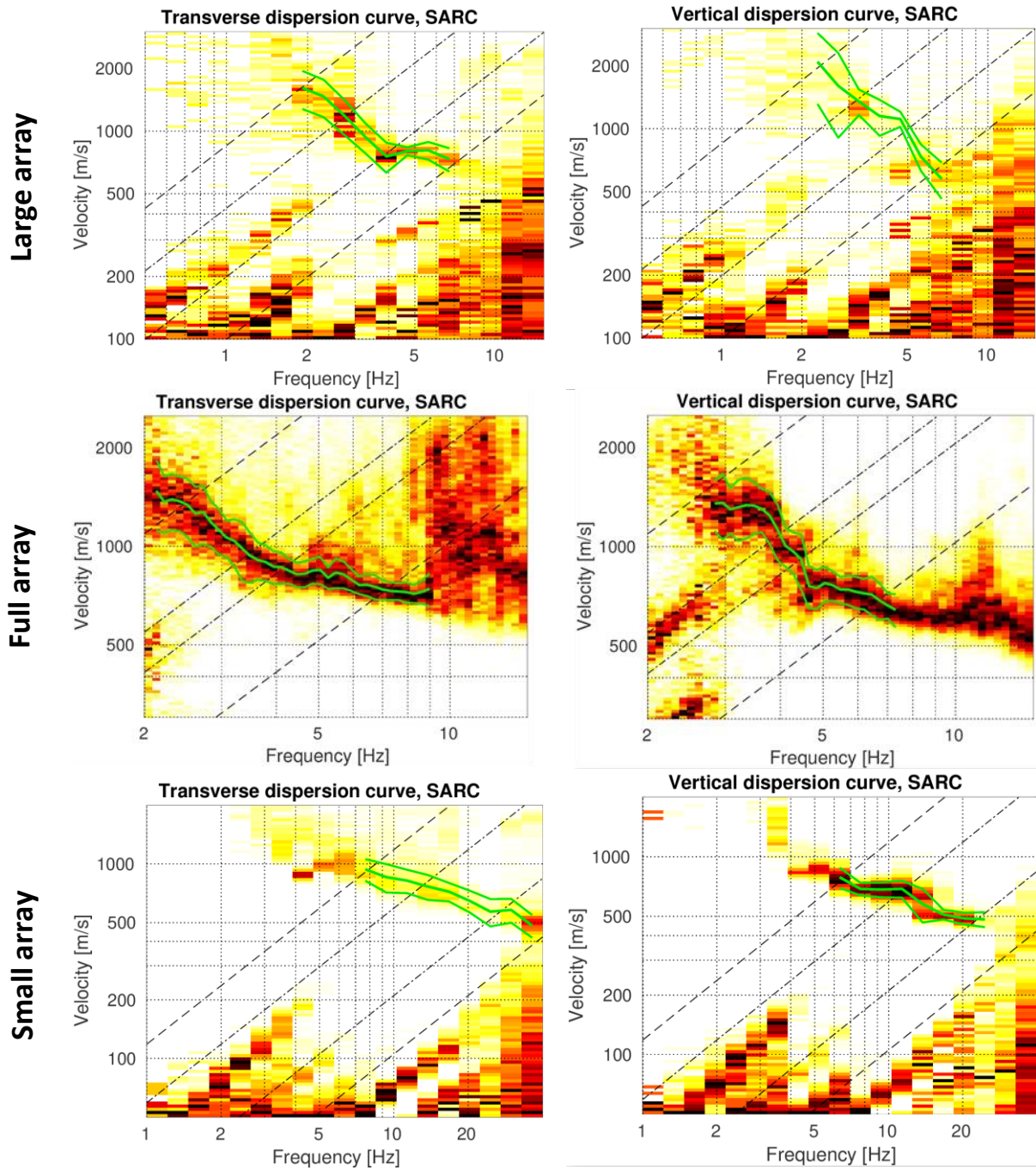
Figure 9: Dispersion curves for the transverse and vertical components obtained with the 3-component HRFK algorithm (Poggi and Fäh, 2010) on the large (top panels), full (central panels), and small arrays (bottom panels). The dashed and dotted black lines are the array resolution limits. The solid green lines are picked from the data, where the central line indicates the best value and the two outer lines the standard deviation, respectively.
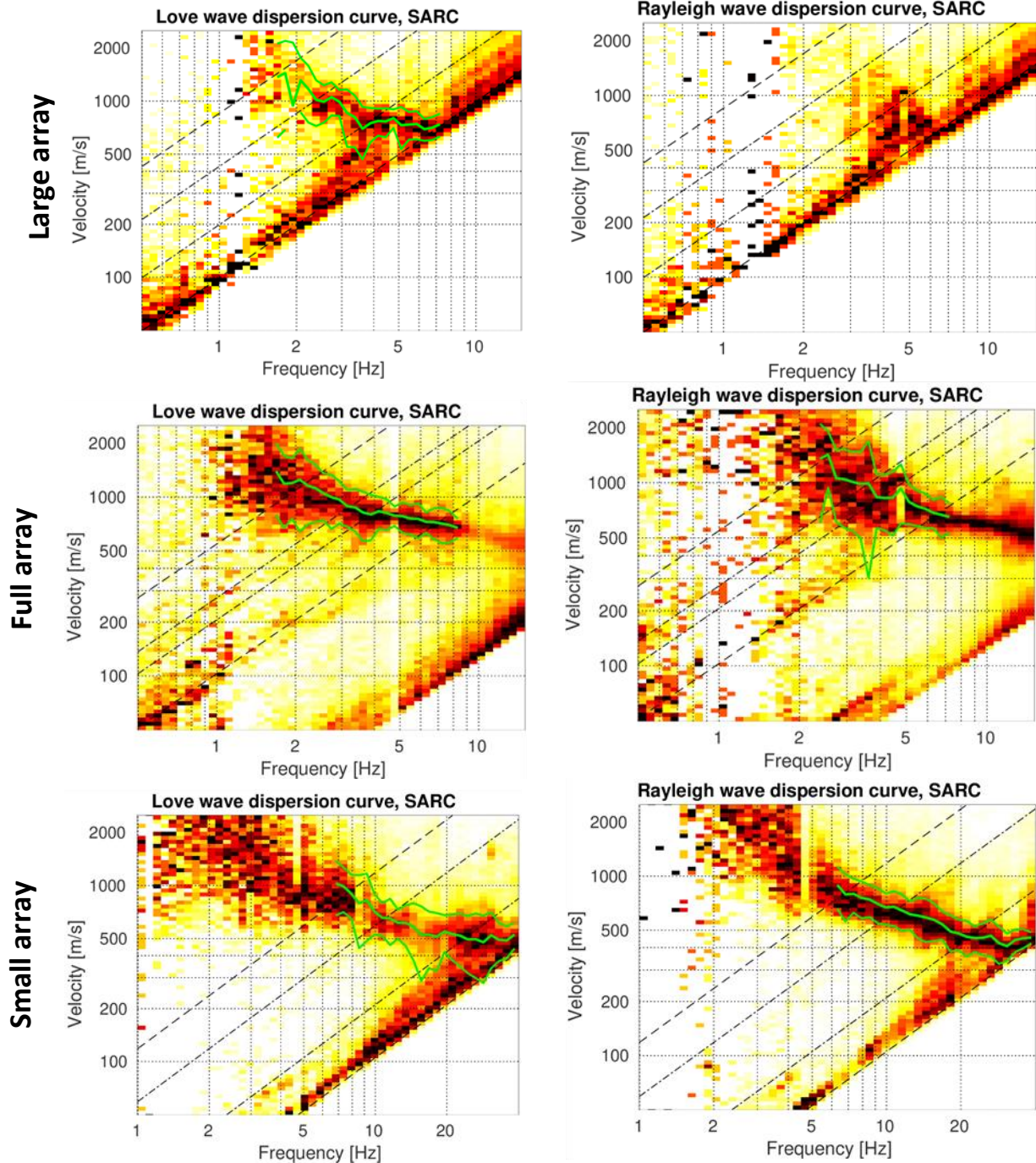
14

Figure 10: Dispersion curves for the Love and the Rayleigh waves obtained with WaveDec (Maranò et al., 2012) on the large (top panels), full (central panels), and small arrays (bottom panels). The solid green lines are picked from the data, where the central line indicates the best value and the two outer lines the standard deviation, respectively.
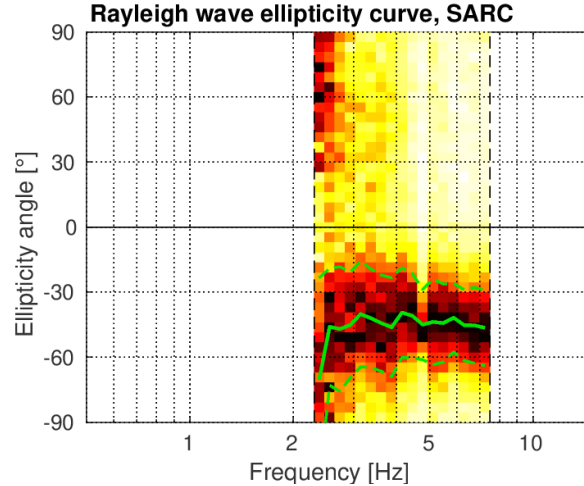
Figure 11: Ellipticity angle for the Rayleigh waves obtained with WaveDec (Maranò et al., 2012) for the full array. The solid green lines are picked from the data, where the central line indicates the best value and the two outer lines the standard deviation, respectively.

4.3 Summary

Figure 12 gives an overview of the dispersion curves determined by the different methods. For Love waves, WaveDec gives a dispersion curve that is in a relatively good agreement with the transverse component of 3HRFK for the large and full arrays. The transverse component of 3HRFK for the small array (above 8 Hz) is not consistent with WaveDec. For the Rayleigh waves, there is also a good agreement between the two different methods (vertical HRFK and WaveDec). However, for both Rayleigh and Love wave dispersion curves, WaveDec indicates lower values than HRFK below 4 Hz. The dispersion curves determined for the small array are shifted towards higher frequencies with respect to the two other arrays.

It was not possible to estimate the ellipticity curve at the peak with the array methods because of the limitation of the array resolution.
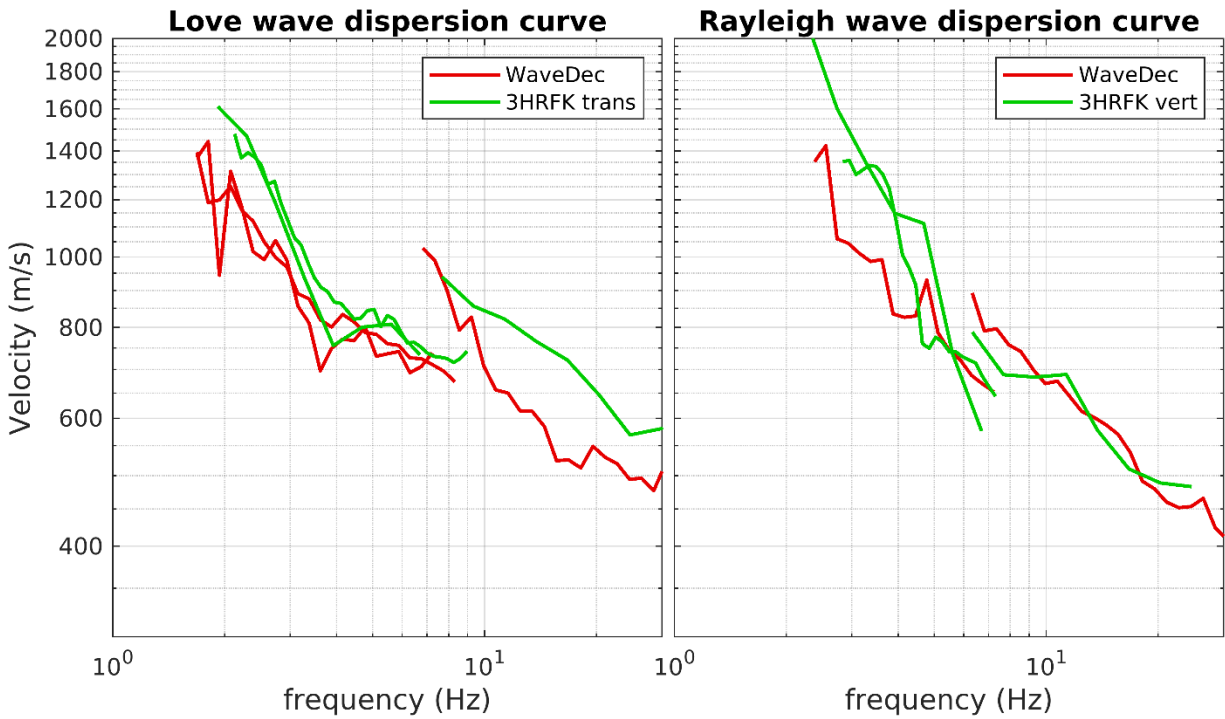
Figure 12: Comparison between the dispersion curves determined by the different methods for the large, the full and the small arrays.

5 Data inversion

5.1 Inversion targets

We performed inversions using as much information as possible, by means of different parts of the picked dispersion and ellipticity curves. The details of these inversion targets are indicated in Table 1 and the corresponding curves are shown in Fig. 13.

In the inversion process, the curve derived with HRFK was used preferentially for Rayleigh waves and at low frequencies (<4 Hz) for Love waves. At higher frequencies, WaveDec was used preferentially for Love wave as it provides more reasonable values for the fundamental mode than HRFK, and it reaches higher frequencies. The inversion process included the WaveDec ellipticity above the peak frequency.
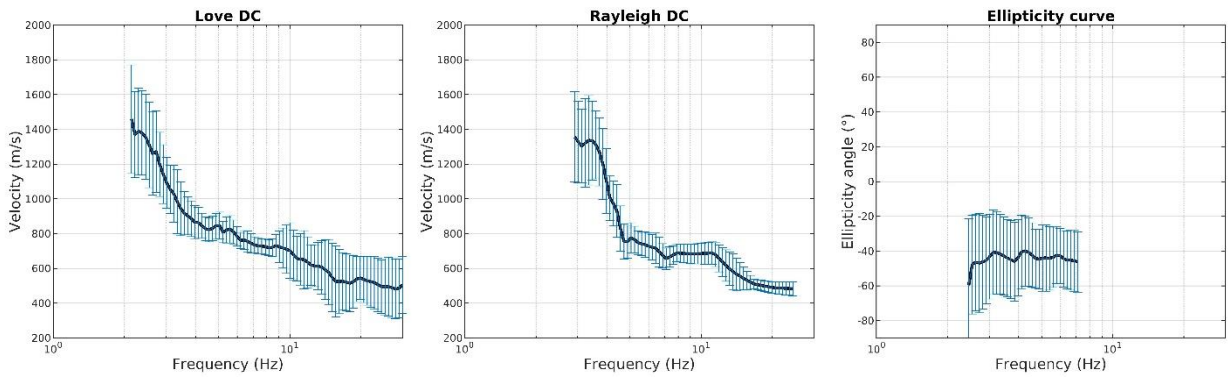

Figure 13: Overview of the dispersion curves used as targets for the different inversions.

Table 1: List of the data curves used as target in the inversion.

Method	Wave type	Mode	Curve type	Frequency range [Hz]
HRFK (T) full array	Love	fundamental	dispersion	2.1 – 8.7
WaveDec small array	Love	fundamental	dispersion	10 – 30
HRFK (V) full array	Rayleigh	fundamental	dispersion	2.9 – 7.1
HRFK (V) small array	Rayleigh	fundamental	dispersion	7.9 – 24.4
WaveDec	Rayleigh	fundamental	ellipticity	2.5 – 7.1

5.2 Inversion parameterization

For the inversion using Dinver (geopsy), four different parameterizations are used in total. They have free values of the depths and velocities of the different layers, ranging from four to seven layers (including half-space).

The S- and P-wave velocities are allowed to range from 150 to 3500 m/s and from 200 to 5000 m/s, respectively. The deepest layer interfaces were allowed to range to a depth of 300 m for all parameterizations. The density was fixed to 2300 kg/m^3 for the bedrock layer and from 1900 to 2100 kg/m^3 for all other layers. No low-velocity zones were allowed in the dinver inversion.

In addition, we invert the data using the new scheme Neopsy (not published yet). This algorithm makes the inversion without any constraint on the number of layers and estimates the probability density function of the inverted parameters. Low-velocity zones were allowed in the neopsy inversion. Identically to Dinver, we used the dispersion and ellipticity curves given in Fig. 13.

5.3 Inversion results

We performed a total of four inversions with Dinver with different parameterizations (see Table 2). Each inversion run produced 200000 total models in order to assure a good convergence of the solution. One inversion was performed using Neopsy. The results of these inversions are shown in Figs 14 – 17.

Table 2: List of inversions

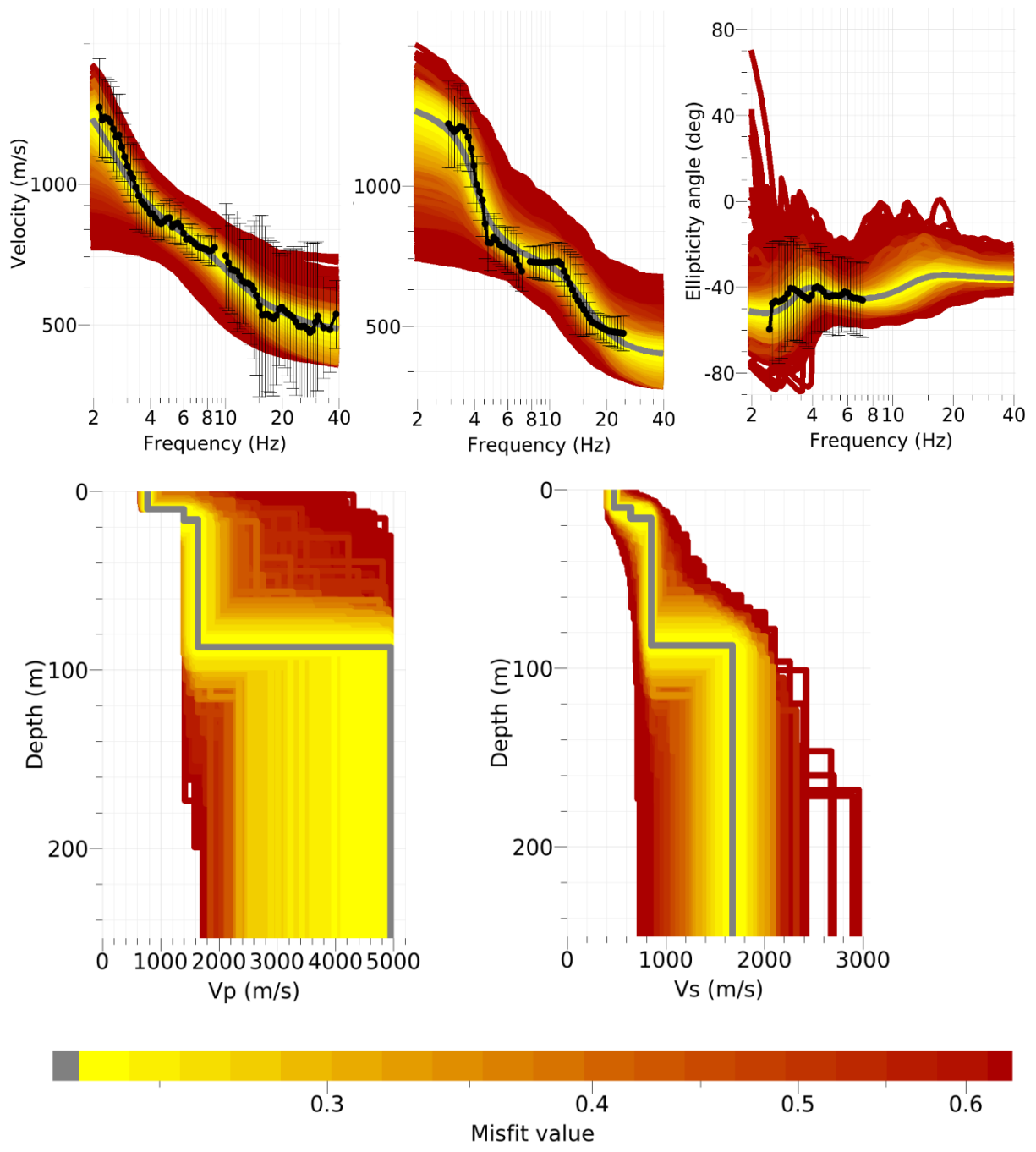| Inversion	Number of layers	Number of models	Minimum misfit
SBUL 4l	4	200000	0.235
SBUL 5l	5	200000	0.235
SBUL 6l	6	200000	0.231
SBUL 7l	7	200000	0.235
Neopsy	unfixed	220000	

Figure 14: Inversion SARC *4l. Dispersion curves for the Love wave fundamental mode (top left) and the Rayleigh wave fundamental mode (top center), Rayleigh wave ellipticity curve (top right), P-wave velocity profiles (bottom left) and S-wave velocity profiles (bottom right). The black dots indicate the data points used for the inversion, the gray line indicates the best-fitting model.*

Figure 15: Inversion SARC 5l. *Dispersion curves for the Love wave fundamental mode (top left) and the Rayleigh wave fundamental mode (top center), Rayleigh wave ellipticity curve (top right), P-wave velocity profiles (bottom left) and S-wave velocity profiles (bottom right). The black dots indicate the data points used for the inversion, the gray line indicates the best-fitting model.*
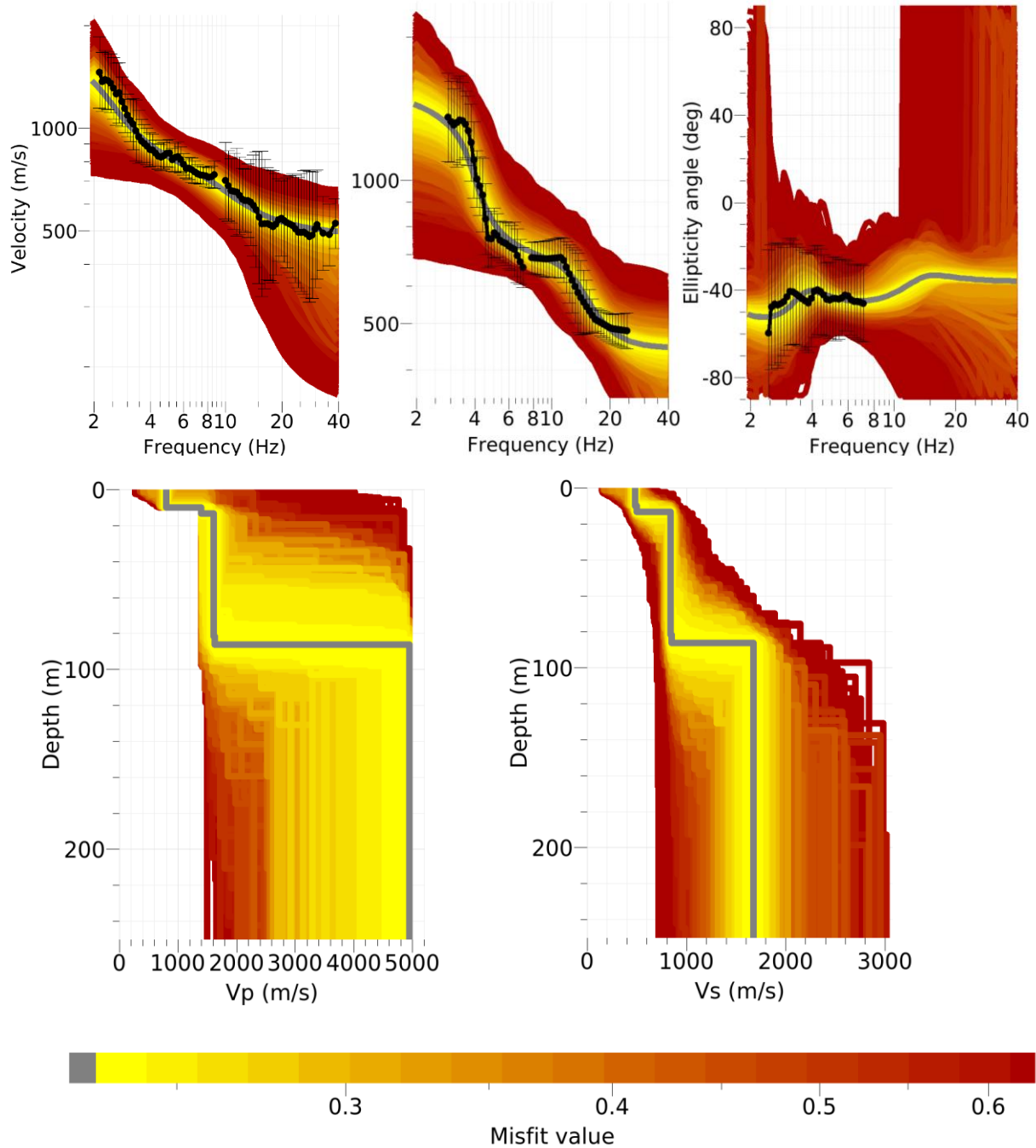
Figure 16: Inversion SARC 6l. *Dispersion curves for the Love wave fundamental mode (top left) and the Rayleigh wave fundamental mode (top center), Rayleigh wave ellipticity curve (top right), P-wave velocity profiles (bottom left) and S-wave velocity profiles (bottom right). The black dots indicate the data points used for the inversion, the gray line indicates the best-fitting model.*
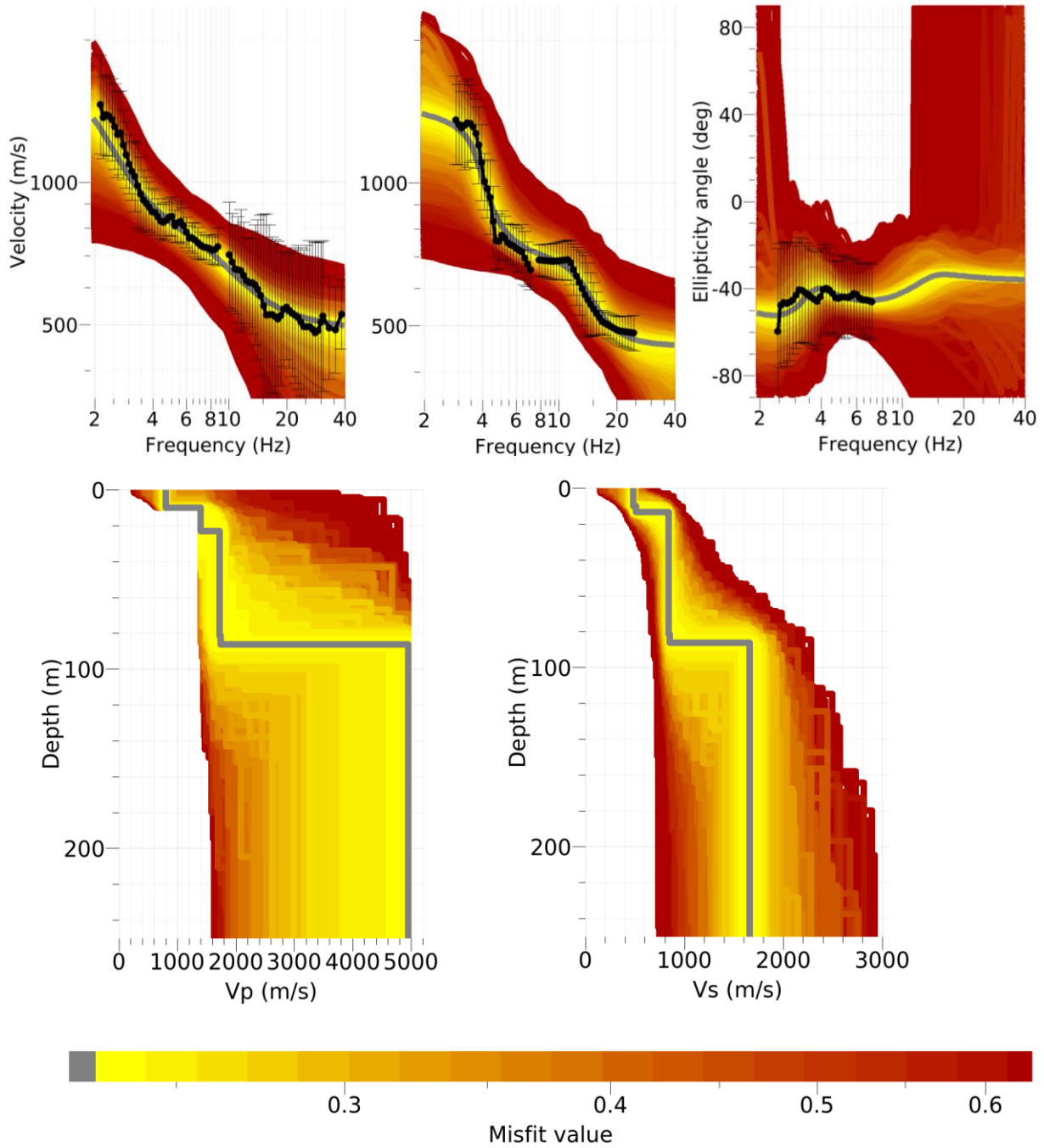
Figure 17: Inversion SARC *7l. Dispersion curves for the Love wave fundamental mode (top left) and the Rayleigh wave fundamental mode (top center), Rayleigh wave ellipticity curve (top right), P-wave velocity profiles (bottom left) and S-wave velocity profiles (bottom right). The black dots indicate the data points used for the inversion, the gray line indicates the best-fitting model.*
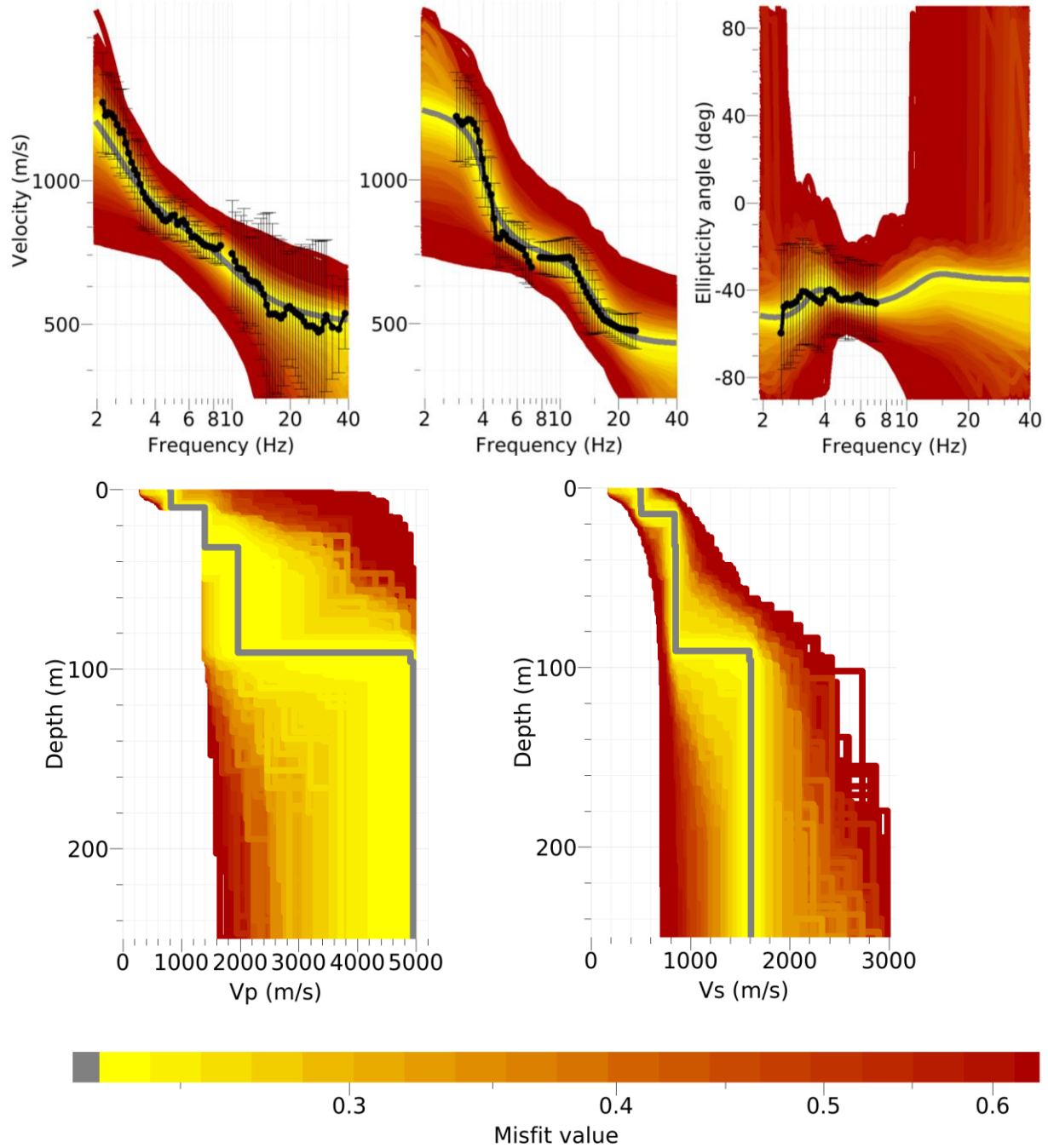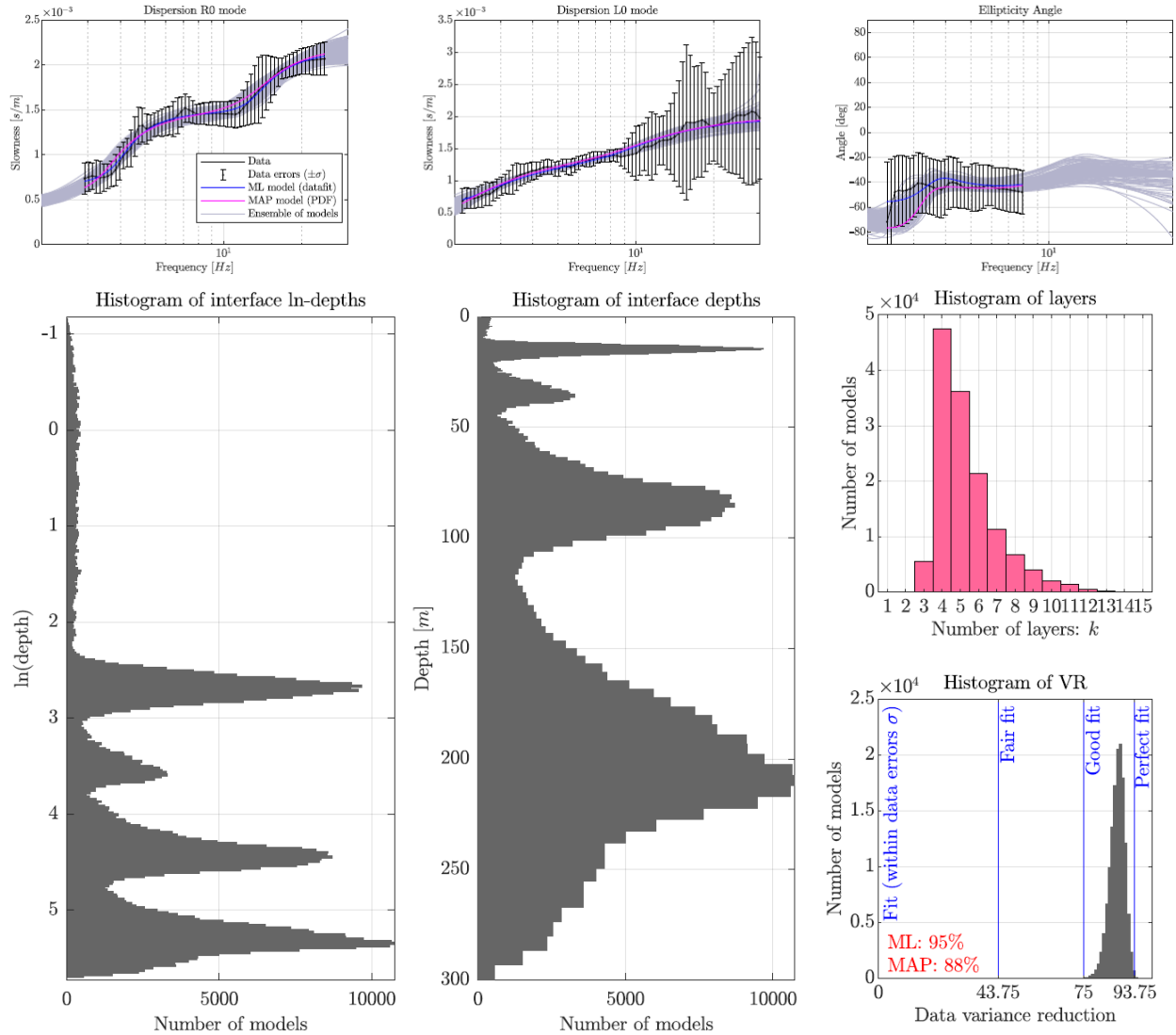
Figure 18: Inversion SARC *Neopsy. Dispersion curves for the Rayleigh wave fundamental mode (top left) and the Love wave fundamental mode (top right). Histogram of interface depths on logarithmic and linear scale (bottom left and center). Histogram of the number of layers and histogram of the variance reduction (bottom right).*
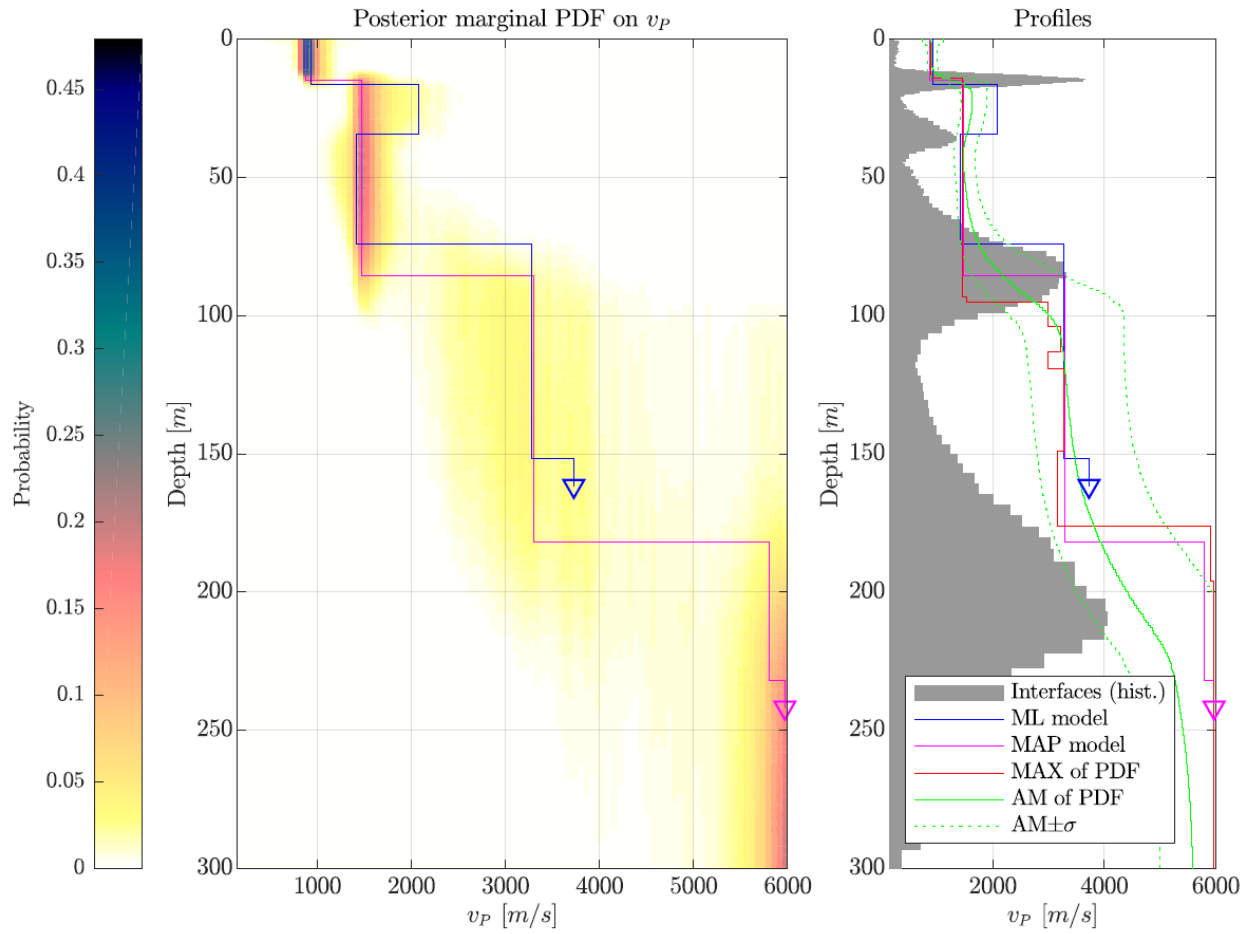
Figure 19: Inversion SARC *Neopsy. Posterior marginal Probability Density Function (PDF - colormap), Maximum Likelihood model (ML - dark blue), Maximum a Posteriori model (MAP - Pink) of Vp.*
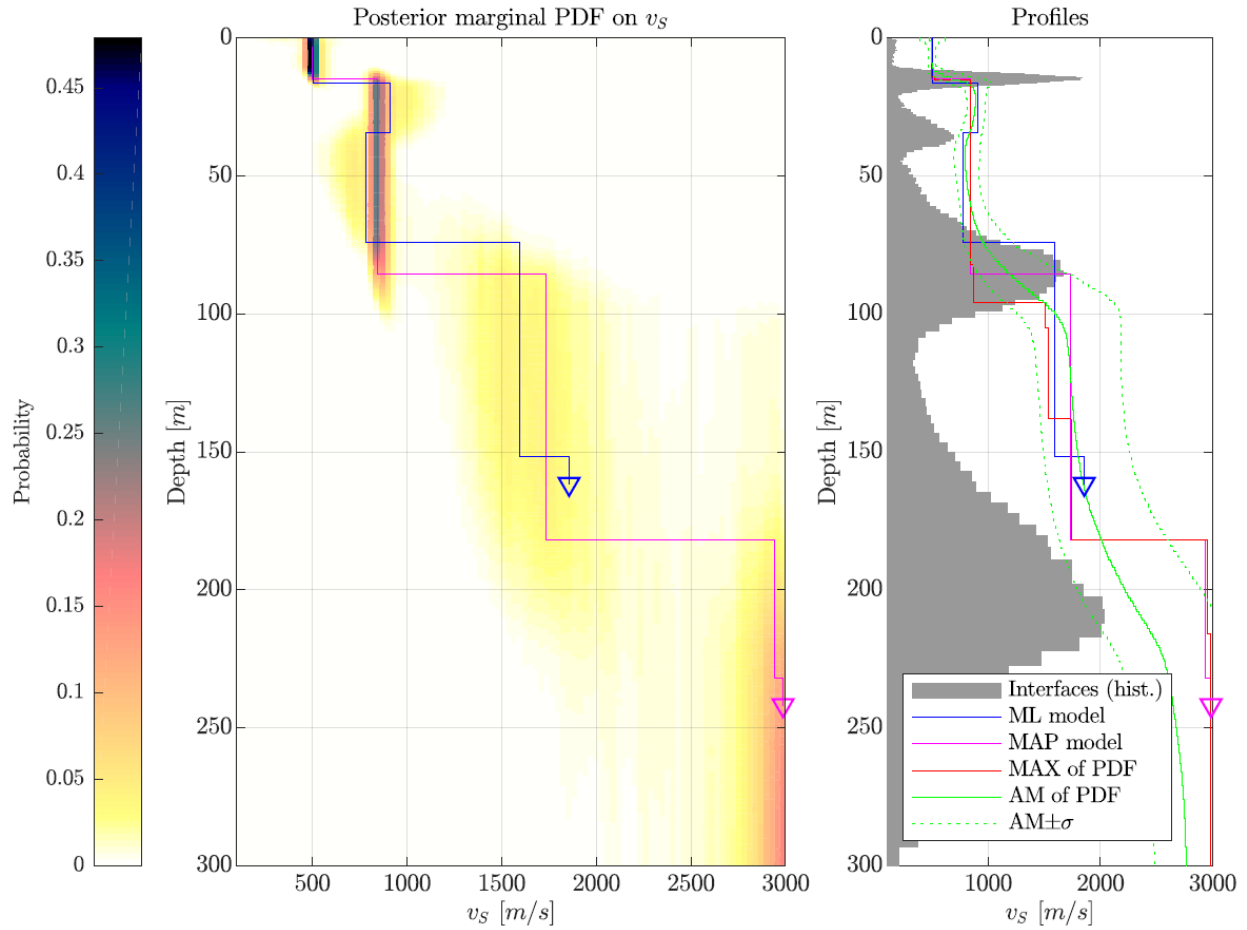
Figure 20: Inversion SARC *Neopsy. Posterior marginal Probability Density Function (PDF - colormap), Maximum Likelihood model (ML - dark blue), Maximum a Posteriori model (MAP - Pink) of Vs.*

5.4 Discussion of the inversion results

The best-fitting models of the inversions are shown in Fig. 21. There are several main characteristics that all models have in common. The seismic bedrock is found at depths between 80 and 90 m, with a shear wave velocity of about 1600 m/s. The variability in depth of this discontinuity is probably due to the lack of information below 2.5 Hz in our experimental curves. Above the bedrock, one main discontinuity is visible depending on the model between 10 and 17 m. The velocity profiles resulting from the different inversions have V_{S30} values between 634 and 640 m/s for Geopsy and between 629 and 639 m/s for Neopsy.
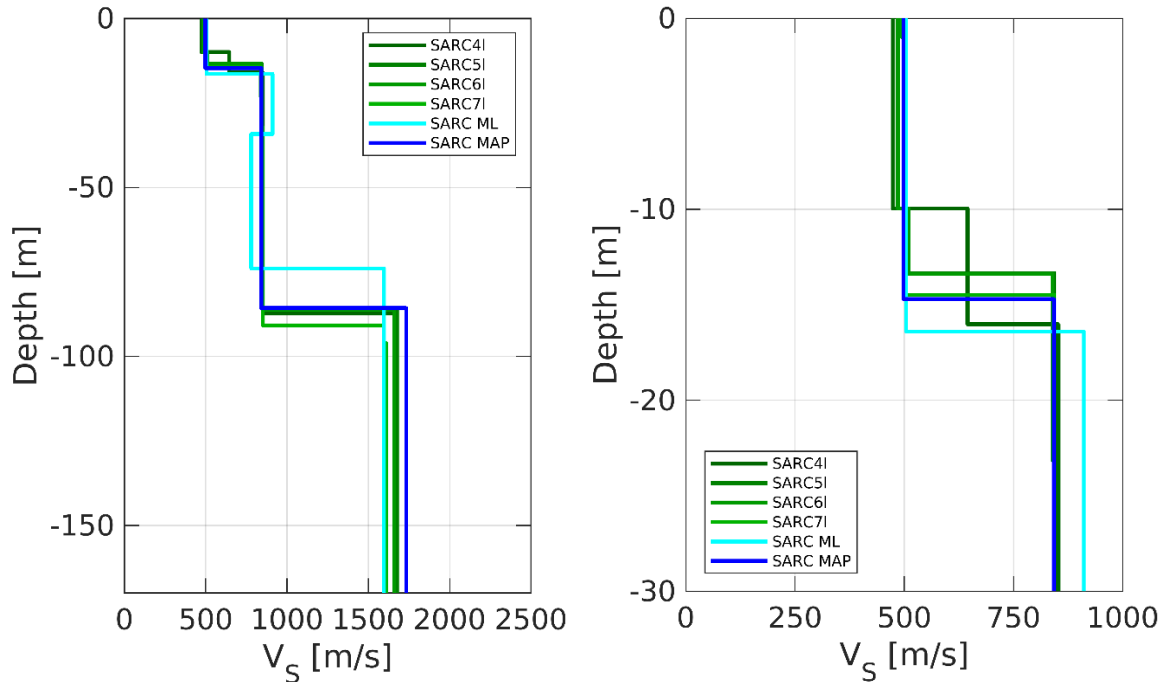

Figure 21: Overview of the shear-wave velocity profiles of the different inversions (left) and zoom on the upper 30 m of the inversion profiles (right).

6 Further results from the inverted profiles

6.1 SH transfer function

In Figure 22, the average theoretical SH-amplification relative to the Swiss reference rock profile from the obtained models is compared to the empirical amplification obtained at station SARC for earthquake recordings (43 earthquakes on 2021-01-19). The models are predicting an amplification up to a factor of 2.5 at about 7.0 Hz, slightly higher than the peak of the empirical amplification. A quite good agreement is observed considering that the station is on the basin-edge. 2D/3D effects are very probably significant and can explain the observed differences.
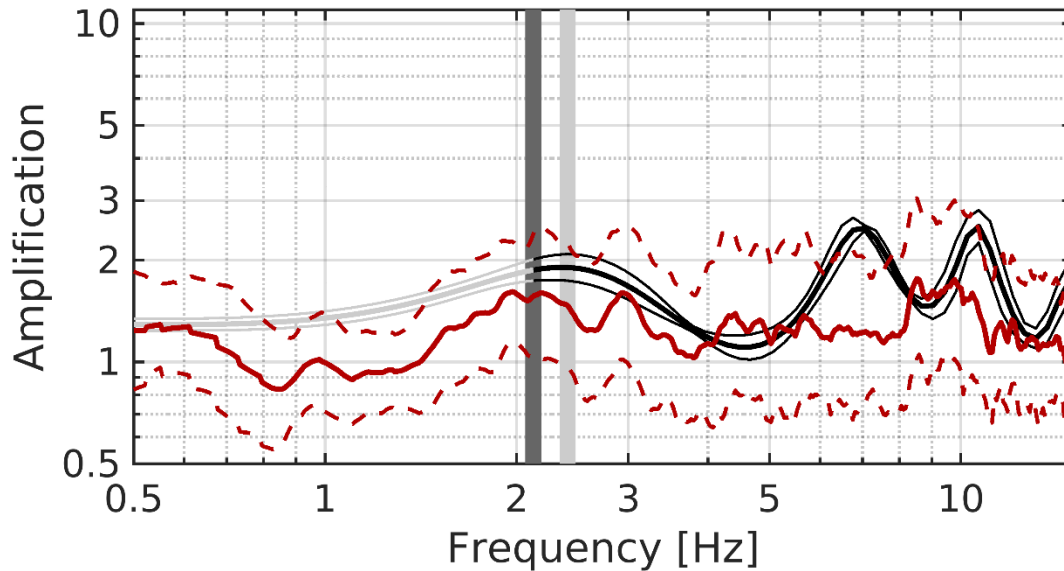

Figure 22: Modeled amplification function computed from the best velocity models of every inversion. The red continuous line is the average empirical amplification function at station SARC, whereas the dashed red lines are the standard deviations. The vertical light and dark grey bars correspond to the lowest frequency of the ellipticity and dispersion curves, respectively.

6.2 Quarter-wavelength representation

The quarter-wavelength velocity approach (Joyner et al., 1981) provides, for a given frequency, the average velocity at a depth corresponding to 1/4 of the wavelength of interest (Fig. 23). It is useful to identify the frequency limits of the experimental data (the minimum frequency of the dispersion curve used in the inversion is 2.1 Hz, the minimum frequency used for the ellipticity inversion 2.5 Hz). The results using this proxy show that the dispersion curves constrain the profiles down to 120 m approximately. The quarter wavelength impedance-contrast introduced by Poggi et al. (2012) is also displayed in the figure. It corresponds to the ratio between two quarter-wavelength average velocities, respectively from the top and the bottom part of the velocity profile, at a given frequency.
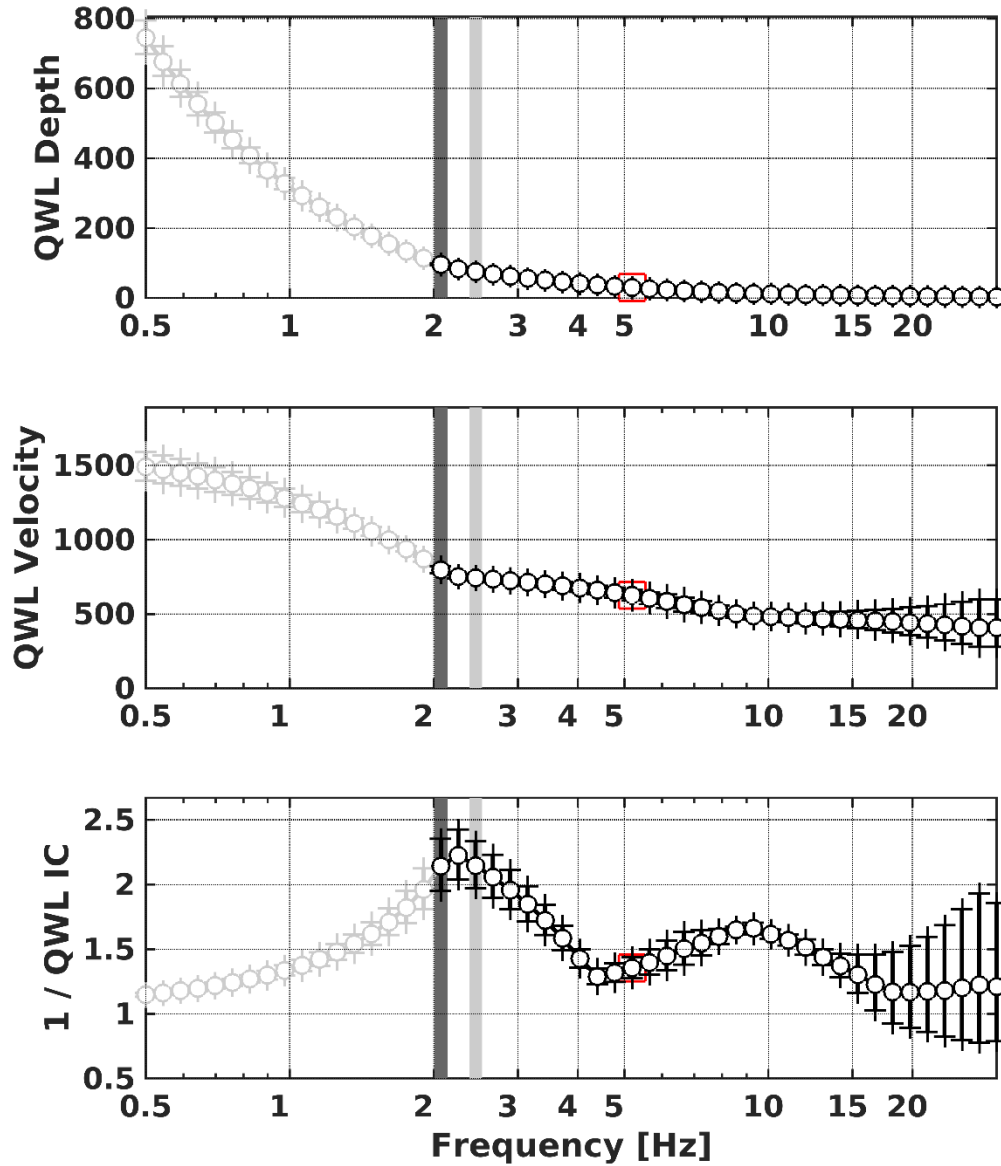
Figure 23: Quarter wavelength representation of the velocity profiles for the best models of the inversions (top: depth, center: velocity, bottom: inverse of the impedance contrast). The grey light bar shows ellipticity lower frequency value, dark grey bar indicates lower frequency value obtained with dispersion curves and red square corresponds to f_{30} (frequency related to the depth of 30 m).

7 Discussion and conclusions

The H/V analysis points out that the fundamental peak observed at the different stations is at about 1.70 Hz, but showing some variability due to the location of the site on the edge of the Rhone valley. The inversion of the passive seismic array measurements yields a velocity profile with two main interfaces at about 10-20 m and 80-90 m. In particular, the upper layer has a velocity of 500 m/s and the second layer is then present with a velocity of about 850 m/s. At about 80-90 m, the velocity jumps to 1600-1900 m/s, very probably related to the bedrock. The V_{S30} value of the site is determined as about 633 m/s, corresponding to soil class B in EC8 and in SIA261 classifications.

The theoretical shear-wave transfer function predicts an amplification factor of 2.5 at about 7.0 Hz, which corresponds to a higher mode of resonance. This amplification function is in a pretty good agreement with the observation despite a probable impact of the basin-edge generated surface waves for this site.

Acknowledgements

References

Burjánek, J., Gassner-Stamm, G., Poggi, V., Moore, J. R., and Fäh, D. (2010). Ambient vibration analysis of an unstable mountain slope. Geophys. J. Int., 180:820–828.

Burjánek, J., Moore, J. R., Molina, F. X. Y., and Fäh, D. (2012). Instrumental evidence of normal mode rock slope vibration. Geophys. J. Int., 188:559–569.

Fäh, D., Gardini, D., et al. (2003). Earthquake Cataloque of Switzerland (ECOS) and the related macroseismic database. Eclogae geol. Helv. 96.

Fäh, D., Wathelet, M., Kristekova, M., Havenith, H., Endrun, B., Stamm, G., Poggi, V., Burjanek, J., and Cornou, C. (2009). Using ellipticity information for site characterisation. NERIES deliverable JRA4 D4, available at http://www.neries-eu.org.

Fritsche, S., Fäh, D., Gisler, M., and Giardini, D. (2006). Reconstructing the damage field of the 1855 earthquake inSwitzerland: historical investigations on a well-documented event Geophys. J. Int. (2006)166, 719–731

Hobiger, M., Bard, P.-Y., Cornou, C., and Le Bihan, N. (2009). Single station determination of Rayleigh wave ellipticity by using the random decrement technique (RayDec). Geophys. Res. Lett., 36.

Maranò, S., Reller, C., Loeliger, H.-A., and Fäh, D. (2012). Seismic waves estimation and wavefield decomposition: Application to ambient vibrations. Geophys. J. Int., 191:175–188.

Poggi, V. and Fäh, D. (2010). Estimating Rayleigh wave particle motion from three component array analysis of ambient vibrations. Geophys. J. Int., 180:251–267.

Poggi, V., Edwards, B., and Fäh, D. (2010). Characterizing the Vertical-to-Horizontal Ratio of Ground Motion at Soft-Sediment Sites. Bulletin of the Seismological Society of America, 102(6): 2741 2756.